International Journal of Heat and Mass Transfer 52 (2009) 3747–3756

Contents lists available at ScienceDirect

International Journal of Heat and Mass Transfer

journal homepage: www.elsevier.com/locate/ijhmt

Suppression of melt convection in a proposed Bridgman crystal growth system

J.A. Wei [a], L.L. Zheng [a,b,*], H. Zhang [c]

[a] Department of Mechanical Engineering, Stony Brook University, Stony Brook, NY 11794, USA
[b] School of Aerospace, Tsinghua University, Beijing 100084, China
[c] Department of Engineering Physics, Tsinghua University, Beijing 100084, China

ARTICLE INFO

Article history:
Received 22 September 2008
Received in revised form 17 February 2009
Accepted 18 February 2009
Available online 7 April 2009

Keywords:
Bridgman technique
Solidification
Compound semiconductors
Modeling
Flow control

ABSTRACT

Numerical simulations are performed for Bridgman crystal growth of several semiconductor materials, such as InAs, InSb, GaSe, CdTe, PbTe, and GaP. For materials with low Prandtl and low Grashof numbers, melt convection is weak and the traditional Bridgman technique is a suitable growth process. For the materials with high Prandtl numbers in their melt status and the growth system with high Grashof number, the temperature field and the growth interface are significantly influenced by melt flow, resulting in the complicated flow pattern and curved interface shape. A new Bridgman crystal growth system is proposed to suppress convection and improve solidification interface shape by cooling of the top melt. The results obtained from the proposed design demonstrate that melt convection may be controlled by adjusting the design parameters. Further, parametric studies are performed to determine the influence of the control parameters on melt flow and solidification interface.

1. Introduction

Vertical Bridgman crystal growth is the dominant technique to grow II–VI and III–V compound semiconductors because of its possibility to maintain low thermal gradient and growth rate independently. When the crystal diameter is small, a virtually flat solidification interface can be maintained due to a weak convection in the melt. As the crystal diameter increases, it is difficult to remove the latent heat from the solidification interface to the crystal sidewall. The temperature difference between the center and the edge of the crystal is therefore large, leading to a curved interface. For the crystal grown with a small Pr number, such as silicon, Ge, GaAs, and InP, convection may not be a serious issue in vertical Bridgman growth, rather the residual convection causing segregation a key issue. However, for the growth of II–VI crystals, such as GaSe and CdTe, the Pr number of its melt is moderate or large, melt flow is actually important since melt flow and thermal transport are strongly coupled and thus melt flow is directly related to dopant uniformity and radial/axial segregation. Strong melt convection could make the interface further curved. In addition, a strong temperature oscillation near the growth interface may cause local instability at the solidification interface, and it may result in polycrystalline growth or twinning formation [1,2]. Suppressing melt convection is therefore needed. On the other hand, weak melt convection may cause axial and radial segregation, e.g., species non-uniformity distribution in the radial and axial directions due to an insufficient mixing. It is therefore important to have the right amount of convection in the melt during crystal growth so that temperature oscillation near the interface can be sufficiently suppressed and species distribution should be uniform. Melt control in the Bridgman crystal growth system is considered as a crucial need for the growth of high quality crystals. In general, it is important to minimize the constitutional undercooling through maintaining a suitable temperature gradient, meanwhile, providing a proper mixing to ensure the impurity piled up at the growth interface being efficiently swept away by melt flow.

Good understanding of heat and mass transfer in the traditional Bridgman crystal growth has been achieved by numerical models [3,4]. However, most work examines the system scaling up for a particular material such as the effect of the Grashof or Rayleigh number on melt flow, temperature distribution, and solidification interface movement. The effect of material properties on heat and mass transfer is less understood. It remains unclear why some crystals are easy to grow and some are not, and why some crystals can grow well with enhanced melt flow and some with suppressed melt flow. Many techniques were designed to control melt convection, including applied magnetic field, accelerated crucible rotation, ampoule tilting, submerged baffle and heater, submerged vibrator, applied electric field, etc. Some techniques are used to enhance heat transfer and others are used to suppress melt flow. Applied magnetic field is a widely used technique for reducing melt flow and temperature oscillation [5]. It unfortunately increases the operational cost significantly. In the submerged methods [6,7], a disk-shaped heater or baffle is held near the

* Corresponding author. Address: School of Aerospace, Tsinghua University, Beijing 100084, China. Tel.: +86 10 6279 7961.
E-mail address: zhenglili@tsinghua.edu.cn (L.L. Zheng).

0017-9310/$ - see front matter © 2009 Elsevier Ltd. All rights reserved.
doi:10.1016/j.ijheatmasstransfer.2009.02.029

Nomenclature

b	inner radius of ampoule (m)
D_{cry}	inner diameter of ampoule (m)
C_p	specific heat (J/Kg K)
g	gravity acceleration (m/s^2)
Gr	Grashof number
H_1	length of hot zone 1 (m)
H_2	length of hot zone 2 (m)
H_{ad}	length of adiabatic zone (m)
H_c	length of cold zone (m)
H_{tr}	length of transition zone (m)
k	thermal conductivity of melt (W/m K)
p	pressure (N/m^2)
Pr	Prandtl number
Ste	Stefan number
t	time (s)
T	temperature (K)
T_c	temperature at cold zone (K)
T_h	temperature at hot zone (K)
T_M	melting point (K)
$\vec{u}$	velocity vector (m/s)
u,v	velocity components in the x and y directions, respectively (m/s)
ΔH_f	latent heat (J/Kg)

Greek symbols

α	thermal diffusivity (m^2/s)
β	thermal expansion coefficient (/K)
δ_{amp}	thickness of ampoule (m)
δ_{gap}	thickness of gap between ampoule and inner surface of furnace (m)
θ	dimensionless temperature
ρ	density of melt (kg/m^3)
μ	viscosity (kg/m s)

Subscripts

a	ampoule
l	melt
s	solid

solid–liquid interface in a traditional Bridgman system. The baffle acts as a partition, separating a small melt zone adjacent to the growth interface from bulk melt. This technique can significantly reduce natural convection near the interface and diffusion-controlled segregation may be resolved [8]. Fedyushkin et al. [9] studied melt flow and solidification interface shape using a submerged vibrator. They found that the thickness of the boundary layer near the interface was decreased, and the solidification front was flattened due to the presence of the submerged vibrator. The submerged baffle or vibrator is also the possible source of contamination. Various methods were also designed to enhance the mixing in the Bridgman growth. Derby and co-workers [10,11] found that a tilting ampoule strongly affected the structure and the strength of melt convection by promoting three-dimensional flow, which in turn modifies heat transfer and the shape of solidification interface. Vizman et al. [12] investigated the effect of a tilted ampoule on melt flow. They concluded that such effect is more significant on semi-transparent material than opaque material. Lan and co-workers [13–16] investigated the effects of an accelerated crucible rotation technique (ACRT) on enhancing melt flow. They found that the ACRT can control the melt flow, but may generate growth striation.

This paper will investigate the role of various dimensionless parameters, such as the Grashof, Prandtl, Biot, and Stefan numbers, on melt flow and temperature distribution in the growth system as well as the solidification interface movement. In particular, the Bridgman crystal growth of six semiconductor materials, such as InAs, InSb, GaSe, CdTe, PbTe and GaP, will be studied. By comparing the difference in dimensionless parameters, the growth of materials will be categorized into a few groups, within each group melt flow and heat transfer behaviors are similar. Numerical simulations are performed to show velocity and temperature fields under the various operating conditions, together with the interface shapes. A new Bridgman growth system is proposed capable of melt control.

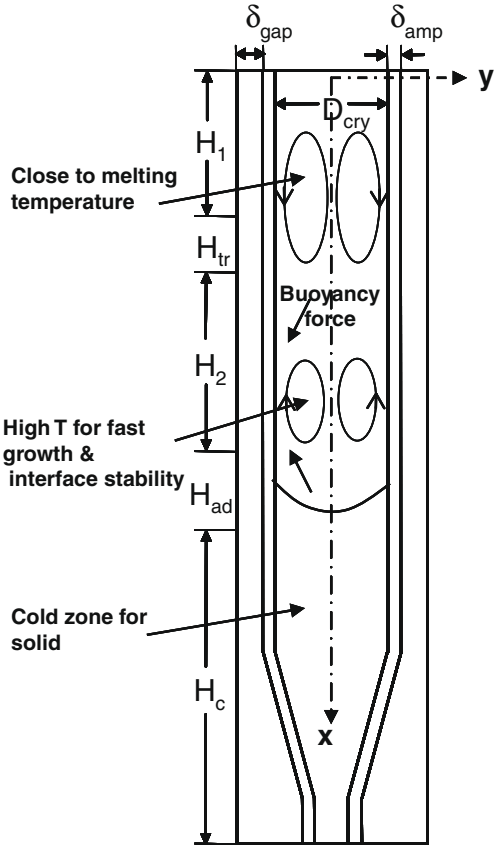

Fig. 1. Schematic of the proposed five zones vertical Bridgman system that differs from the traditional three zones furnace in which only one hot zone represented by the length H_h is present instead of ($H_1 + H_{tr} + H_2$).

2. System configuration and mathematical formulation

A traditional Bridgman system is schematically shown in Fig. 1(a). It consists of hot, cold and adiabatic zones with the heights of H_h, H_c and H_{ad}, respectively. And the ampoule with sample is position inside the furnace vertically. The crystal diameter (ampoule's inner diameter) is D_{cry}, the ampoule wall thickness is δ_{amp} and the gap between ampoule and furnace is δ_{gap}. The charge is first loaded into the ampoule and heated to a temperature above the melting temperature. After the system is thermally stable, the furnace (or ampoule) is then moved upwards (or downwards) and the molten melt is solidified. T_h, T_c and T_M represent the temperatures at the hot and cold zones, and at the melting point, respectively. The solidification interface undergoes dynamic evolution and its moving

speed changes with time in the beginning and may reach a constant speed afterwards. Thus the problem or geometry itself is time-dependent. To reflect the growth experiments, we simulate the growth method, in which the sample is stationary and the furnace is moving at a given speed (pull rate). The computational domain includes the sample with ampoule and the moving thermal boundary has been applied to the outside of the ampoule. Since the main objective of this paper is to investigate the flow motion and thermal transport affected by the growth materials in terms of their Prandtl numbers, we simplify the seeding process by assuming that the growth is initially after the system reaches thermal equilibrium with the portion of material in solid and portion of that in melting status. The interface shape has also reached the steady location with no pull rate. With this initial condition, the system is then simulated with transient equations and a constant pull rate. To simulate the Bridgman growth, the following assumptions are made: (a) melt flow is incompressible, laminar, and axisymmetric; (b) melt is the Newtonian fluid; and (c) thermo-physical properties are assumed to be constant for the given phases. With the above assumptions, the governing equations can be written as follows:

For the melt:

$$\text{Continuity equation}: \quad \nabla\cdot(\rho_l\vec{u}) = 0 \tag{1}$$

$$\text{Momentum equation}: \quad \frac{\partial}{\partial t}(\rho_l\vec{u}) + \nabla\cdot(\rho_l\vec{u}\vec{u}) = -\nabla p + \mu_l\nabla^2\vec{u} + \rho_l\vec{g} \tag{2}$$

$$\text{Energy equation}: \quad \frac{\partial}{\partial t}(\rho_l C_{pl}T) + \nabla\cdot(\rho_l C_{pl}T\vec{u}) = \nabla\cdot(k_l\nabla T) \tag{3}$$

For the solid (crystal and ampoule):

$$\text{Energy equation}: \quad \frac{\partial}{\partial t}(\rho_s C_{ps}T) = \nabla\cdot(k_s\nabla T) \tag{4}$$

At the solidification interface

$$\text{Energy balance}: \quad -k_s\frac{\partial T}{\partial n}\Big|_s + k_l\frac{\partial T}{\partial n}\Big|_l = \rho_l\Delta H_f u_n \tag{5}$$

where ρ, C_p and k are the density, specific heat capacity and thermal conductivity, respectively, ΔH_f is the latent heat. The subscripts s, l, and n represent solid, liquid and the direction normal to the interface, respectively. In this paper, simulation is only conducted for flow with laminar type including oscillation regime. The suitable growth conditions have been selected so that the flow will not exhibit transition to turbulence.

To determine the role of the dimensionless parameters, the governing Eqs. (1)–(5) are non-dimensionalized. The reference scales include the length scale by the inner radius of the ampoule, b, velocity scale by the ratio of kinematic viscosity, ν_l, to reference length scale, and the temperature scale (ΔT) by the temperature difference between the high temperature T_h and the melting temperature T_m. Specifically, the non-dimensional parameters are defined as $x' = x/b, y' = y/b, u' = ub/\nu_l, t' = t\nu_l/b^2, p' = (p-\rho_l g x)/(\rho\nu_l^2/b^2), \theta = (T-T_M)/\Delta T$, and $k' = k/k_l$. The dimensionless forms of the governing Eqs. (1)–(5) are obtained as follows,

$$\nabla\cdot\overrightarrow{u'} = 0, \tag{6}$$

$$\frac{\partial\overrightarrow{u'}}{\partial t'} + \nabla\cdot\left(\overrightarrow{u'}\overrightarrow{u'}\right) = -\nabla p' + \nabla^2\overrightarrow{u'} - Gr\theta\vec{i}_g, \tag{7}$$

$$\frac{\partial\theta}{\partial t'} + \nabla\cdot\left(\theta\overrightarrow{u'}\right) = \frac{1}{\mathrm{Pr}}\nabla^2\theta, \tag{8}$$

$$\frac{\partial}{\partial t'}\left(\rho_s' C_{ps}'\theta\right) = \frac{1}{\mathrm{Pr}}\nabla\cdot(k_s'\nabla\theta), \tag{9}$$

$$-\frac{k_s}{k_l}\frac{\partial\theta}{\partial n}\Big|_s + \frac{\partial\theta}{\partial n}\Big|_l = \frac{\mathrm{Pr}}{Ste}u_n', \tag{10}$$

In Eq. (7), $\vec{i}_g$ is the unit direction of gravity force. Here it is assumed positive when it is in the positive direction of the coordinate. The dimensionless parameters include the Grashof number, $Gr = \beta\Delta T g b^3/\nu_l^2$, the Prandtl number, $\mathrm{Pr} = \nu_l/\alpha_l$, and the Stefan number, $Ste = C_{pl}\Delta T/\Delta H_f$. The Grashof number is the most important parameters in the melt flow and it represents the strength of melt convection caused by natural convection. The Prandtl number is a parameter representing the coupling between fluid flow and thermal transport and it indicates the influence of melt convection on temperature distribution and solidification interface shape. The Stefan number is related to the latent heat release, consequently the movement of the solidification interface. If the latent heat released from the solidification cannot be taken out efficiently in the solid crystal, a curved interface is usually resolved.

3. Boundary/initial conditions and numerical method

The numerical region covers the sample (both solid and liquid), ampoule and the gas medium in between the ampoule and furnace. With respect to the coordinate system in Fig. 1, the boundary conditions for temperature and velocity are specified as follows:

at the central axis, $y' = 0$:

$$\frac{\partial\theta}{\partial y'} = 0, \ \frac{\partial u'}{\partial y'} = 0, \quad \text{and} \quad v' = 0$$

at the interface between the gas medium and the furnance, $y' = (b + \delta_{amp} + \delta_{gap})/b$:

$$\begin{aligned} &\theta = 1 && \text{if} \quad \hat{x} \leqslant (H_1 + H_{tr} + H_2)/b \\ &\theta = 0 && \text{if} \quad (H_1 + H_{tr} + H_2) < \hat{x} \leqslant (H_1 + H_{tr} + H_2 + H_{ad})/b \\ &\theta = (T_c - T_m)/\Delta T && \text{if} \quad \hat{x} > (H_1 + H_{tr} + H_2 + H_{ad})/b \end{aligned}$$

at the ampoule inner and out walls, $y' = 1$ and $y' = (b + \delta_{amp})/b$:

$$u' = 0 \quad \text{and} \quad v' = 0$$

at the top of the sample, $x' = 0$:

$$\frac{\partial\theta}{\partial x'} = 0, \ \frac{\partial u'}{\partial x'} = 0, \quad \text{and} \quad v' = 0$$

at the solidification interface, x'_{int}:

$$\theta = 0.$$

To mimic the actual experiment, the temperature profile at the interface between the gas medium and furnace will move at the pull rate. Note that at the solidification interface, the heat flux balance obeys Eq. (10) in addition to the temperature constraint of the melting point. The initial temperature distributions in the solid, melt and ampoule are the simulation results for the steady-state condition with the above given temperature profile.

The governing equations for mass, momentum and energy Eqs. (6)–(10) have been solved using the adaptive curvilinear finite volume scheme (MASTRAPP) developed by Zhang and Moallemi [17] and Zhang et al. [18] and improved by Zheng et al. [19]. The melt flow pattern and heat transfer in the crystal growth system are predicted. The principle components of this scheme include multizone adaptive grid generation (MAGG) and curvilinear finite volume approach (CFV) and grid migration. This numerical scheme is capable of capturing the interface shape and location efficiently since the solid/melt interface is tracked explicitly using the multizone adaptive grid generation scheme which ensures sufficient fine grids near [17–22].

Table 1
Thermophysical properties of InAs, GaP,InSb, PbTe, CdTe and GaSe.

Property	InAs	GaP	InSb	PbTe	CdTe	GaSe
Melting point, T_M, K	1215 [23]	1730 [14]	800 [23]	1190 [14]	1365 [24]	1210 [25]
Enthalpy of fusion, ΔH_f, J/kg	405.74×10^3	706.1×10^3 [26]	206.0×10^3 [27]	342.3×10^3 [19]	209.2×10^3	376.6×10^3 [25]
Thermal expansion coefficient, β, /°C	4.07×10^{-5} [28]	4.65×10^{-4} [14]	1.0×10^{-4} [23]	2.13×10^{-4} [14]	5.0×10^{-4}	1.287×10^{-4} [25]
Density, ρ, kg/m³						
Melt	5890 [23]	4562 [14]	6480 [23]	7450 [14]	5640 [19]	4814 [25]
Crystal	5500 [23]	4138 [14]	5760 [23]	8160 [14]	6200 [19]	4930 [25]
Thermal conductivity, k, W/m K						
Melt	13.692	13.0 [30]	17.873	4.18 [14]	2.0 [24]	0.756 [25]
Crystal	5.477 [29]	5.2 [30]	7.30 [29]	3.11 [31]	1.0 [24]	0.366 [25]
Specific heat, C_p, J/kg K						
Melt	297.6	482 [14]	280 [23]	200 [32]	187 [18]	560 [25]
Crystal	288 [13]	430 [14]	238 [23]	165 [32]	160 [18]	340 [25]
Kinematic viscosity, ν, m²/s						
Melt	1.75×10^{-7} [23]	4.5×10^{-7} [14]	3.70×10^{-7} [23]	6.790×10^{-7} [14]	8.0×10^{-7}	7.81×10^{-7} [25]
Dynamic viscosity, μ, kg/m s						
Melting point	1.02×10^{-3} [23]	2.05×10^{-3} [14]	2.400×10^{-3} [23]	5.059×10^{-3} [14]	4.51×10^{-3} [3]	3.76×10^{-3} [25]
Thermal diffusivity, α, m²/s						
In the melt	7.81×10^{-6}	5.91×10^{-6} [14]	9.85×10^{-6} [23]	2.80×10^{-6}	1.89×10^{-6}	2.80×10^{-7} [25]

4. Results and discussion

4.1. Effect of the control parameters

Six materials GaSe, InSb, InAs, CdTe, PbTe and GaP are studied. To examine the effects of material properties, the geometry and operating conditions are fixed. A 14mm diameter crystal is used as the baseline case. The hot zone temperature is assumed to be 75 °C higher than the melting point. Thermophysical properties of GaSe, InSb, InAs, CdTe, PbTe and GaP crystals are summarized in Table 1. The gap between the ampoule and the inner wall of the furnace is filled with gas being heated by furnace through conduction and radiation. The radiation heat transfer between the outer surface of the ampoule and the inner surface of the furnace is strong. An effective thermal conductivity is assigned to the gap considering radiation with the emissivity of the solid as 0.5. For the system considered here, the melt motion is primarily due to the temperature difference induced natural convection and no rotation is considered in the ampoule. In the crystal growth experiments, a slow rotation rate is usually applied, which is mainly used for the uniformity of heating. The rotational effect will be minimized when the ratio of the square of the rotational Reynolds number to the Grashof number is much smaller than unity. To analyze the key control parameters, the Grashof, Prandtl, Stefan, and Biot numbers are calculated based on a 14 mm diameter crystal with the reference temperature difference of 75 K for the aforementioned six representative II–VI crystal and summarized in Table 2. It is believed that for a crystal growth under the conditions of small Prandtl number e.g., Pr < 0.1 and Grashof number, e.g. Gr < 10^5, the crystal can be grown successfully using the traditional Bridgman system. Melt flow is primarily driven by the interface movement and is not significantly affected by temperature distribution. The temperature distribution is close to the conduction case due to weak convection. For a crystal with high Prandtl number and/or high Grashof numbers, melt flow, temperature field and growth interface are strongly coupled. The shape and the movement of the solidification interface will be affected by many effects. For example, the growth interface shape can be changed from the convex to concave shape by changing the growth rate. In this case, melt convection will have a strong influence on the growth process.

To examine the response of the crystal growth to the materials system, the simulations were conducted for two representative II–VI crystals, InAs and CdTe. Fig. 2 shows the computational grids. Fig. 3 shows the temperature variations along the centerline of the ampoule for InAs and CdTe for the cases with (solid line) and without convection (dash line). The difference between the solid and dashed lines indicates the influence of melt convection on temperature distribution. When the Prandtl number is small, such as InAs, the effect of temperature field on the melt flow is not significant. The temperature profiles with and without convection are similar. When the Prandtl number is large, such as CdTe, the difference of temperature profiles with and without convection becomes obvious, confirming a strong dependence of temperature on melt convection for large Prandtl number.

The simulations have also performed for six II–VI materials. The predicted temperature and velocity distributions are shown Fig. 4

Table 2
Effects of Prandtl, Grashof and Stefan numbers on interface curvature for a crystal size of 14 mm in diameter and the reference temperature difference of 75 °C.

Material	InAs	GaP	InSb	PbTe	CdTe	GaSe
Prandtl number, Pr	0.022	0.03	0.038	0.24	0.42	2.78
Grashof number, Gr	3.35×10^5	5.8×10^5	1.85×10^5	1.16×10^5	2.0×10^5	5.32×10^4
Stefan number, Ste	0.055	0.051	0.21	0.044	0.067	0.11
Ste/Pr	2.5	1.7	2.76	0.18	0.156	0.04
Biot number, Bi	0.24	0.74	0.048	0.39	1.86	3.50
k_s/k_l	0.40	0.39	0.41	0.74	0.50	0.48
k_a/k_l	0.19	0.20	0.14	0.62	1.30	3.44
Rayleigh number, Ra	7.37×10^3	1.74×10^4	7.03×10^3	2.78×10^4	8.4×10^4	1.48×10^5
Interface curvature, δ	0.065	0.15	0.048	0.45	0.63	1.38

Notes: k_s, k_l and k_a are thermal conductivities of crystal, melt and ampoule, respectively. δ is the dimensionless height difference between the points at centerline and inner ampoule wall at the interface.

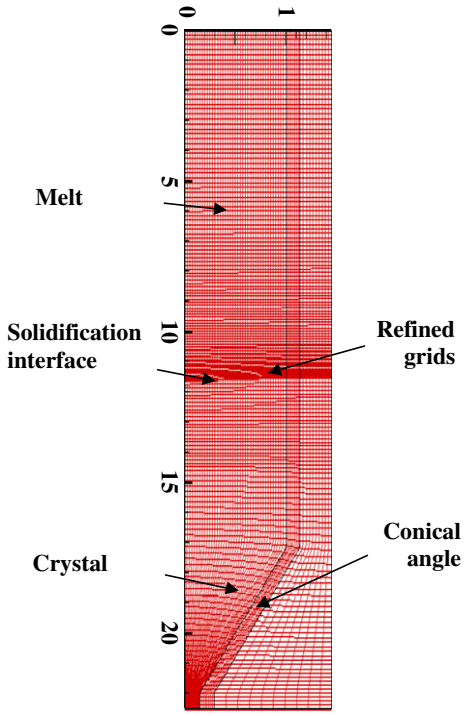

Fig. 2. Numerical grids for a computational domain.

and the interface shapes are summarized in Fig. 5. It is seen that the interface shape becomes more curved as the Prandtl number increases. When the Prandtl number is relatively large, the system with a high Grashof number will experience a strong interplay between the melt convection and solidification. Melt convection becomes stronger when the Grashof number increases. The melt flow may change from laminar to turbulent. The effects of Prandtl, Grashof and Stefan numbers on the interface curvature have been summarized in Table 2. It is noted that the interface evolution is mathematically determined by the dimensionless Eq. (10). It is known that the interface curvature in a vertical Bridgman system is strongly influenced by the rate at which the latent heat released from solidification is transferred away from the interface through the solid crystal. This rate can be described by the dimensionless parameter Ste/Pr and Biot number. The interface is more curved when the value of Ste/Pr is decreased. As the Grashof number increases, the interface shape is more curved, which can be explained by the effect of strong convection. These results also indicate that the temperature distribution is strongly affected by the length of the adiabatic zone for the growth of high Prandtl number crystal, e.g., CdTe and GaSe.

4.2. Effect of crystal diameter

To investigate the effect of crystal diameter, we focus on one material with a fixed Pr number, e.g., CdTe crystal growth. As the crystal diameter increases, the Grashof number in the growth system increases. The Grashof number for the small crystal with 14 mm in diameter is at the order of magnitude of 2.0×10^5, indicating melt flow as laminar. By increasing the crystal size to 25.4 mm, the Grashof number is increased to 1.18×10^6, which is in the transitional region. The melt convection is intensified and an intensified melt flow may disturb the growth interface. If the crystal size is further increased to 38 mm, the Grashof number reaches 4.0 × 106, the melt flow is in the turbulence region. Under this condition, the temperature distribution and solidification interface will be influenced strongly by melt flow. It has been commonly understood that reducing the melt convection and minimizing the temperature fluctuation at the growth interface will be beneficial to the growth.

Fig. 6 shows the predicted streamline and temperature distribution for the growth of CdTe crystal with the diameter of 38 mm in an enlarged view around the growth interface. Due to the relatively large Prandtl number, the temperature distribution in the CdTe growth system is strongly influenced by melt convection, causing unstable growth (interface) condition. Therefore, the improvement on the growth system design or suppressing melt convection is required to grow larger diameter crystals (>50 mm).

4.3. Proposed growth system

As discussed in the previous section, the hot zone temperature boundary condition is important for melt flow. To improve the growth condition, a new design is proposed. The proposed Bridgman system shown in Fig. 1 consists of two hot zones with the heights of H_1 (hot zone 1) and H_2 (hot zone 2), respectively, a transition, an adiabatic and a cold zone with the heights of H_{tr}, H_{ad} and H_c, respectively. The ampoule that holds the crystal has the thickness of δ_{amp} and the gap between the ampoule's external wall and the furnace inner surface is δ_{gap}. The hot zone 1 has the

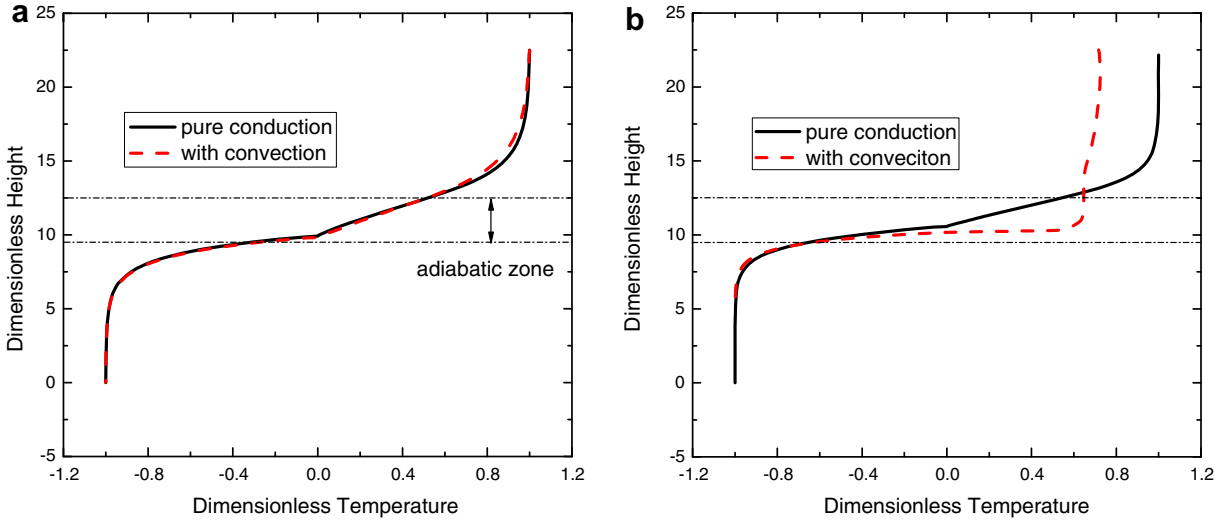

Fig. 3. Temperature profile along the centerline with or without convection for the representative II–VI crystals (a) InAs, and (b) CdTe.

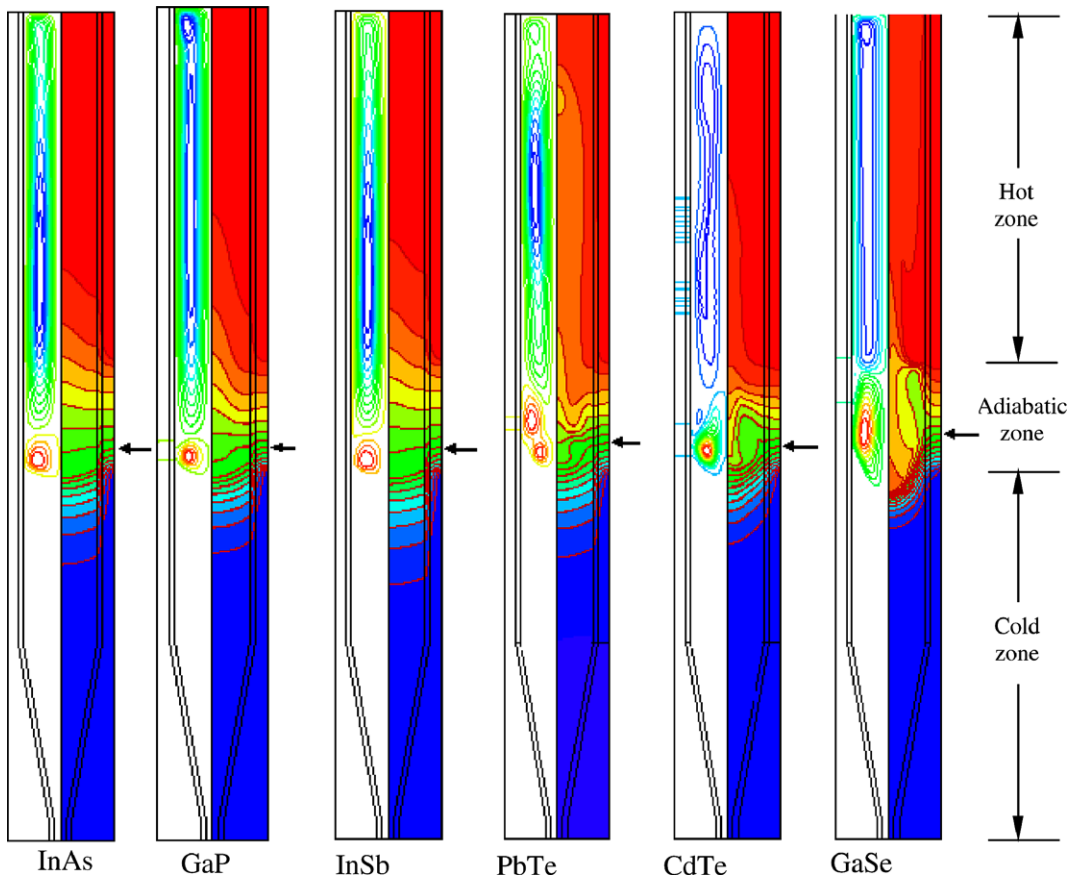

Fig. 4. Streamline (left half) and temperature (right half) distributions during the growth of InAs, GaP, InSb, PdTe, CdTe and GaSe crystals with the diameter of 14 mm.

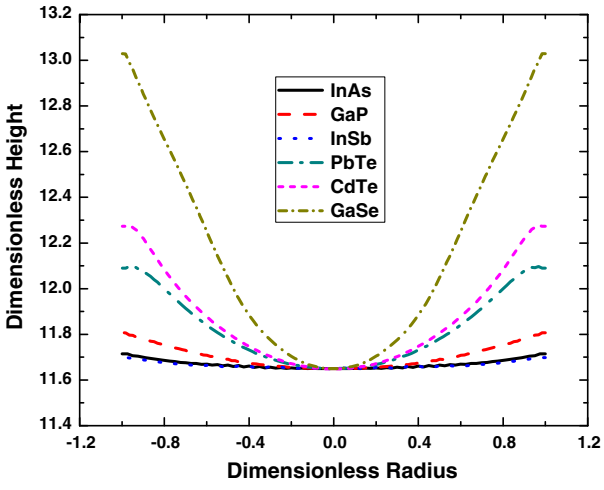

Fig. 5. Solidification interface shapes for the growth InAs, GaP, InSb, PbTe, CdTe and GaSe six II–VI crystals.

temperature slightly above the melting point to ensure no freezing on the wall and the hot zone 2 will have a high temperature for establishing a certain temperature gradient to facilitate growth together with the given cold zone temperature. We will use InSb as an example to illustrate the efficiency of the proposed system and investigate whether two-hot zone design can suppress melt convection efficiently. It is expected the geometric parameters such as H_{tr} , H_2 and H_{ad} will determine the melt flow level. To examine the effects of geometry sizes of different zones, the parametric study is performed here.

The baseline case for the studies in this section has the geometry size of $H_2/D_{cry} = 1$, $H_{tr}/D_{cry} = 0.5$ and $H_{ad}/D_{cry} = 1$, and the crystal size is 38 mm. The streamline and temperature distribution for this case is shown in Fig. 7. To examine the effect of hot zone length H_2 on the growth, the predicted temperature and stream function distributions are presented in Fig. 8 for hot zone size of $H_2/D_{cry} = 5$. When the length of hot zone is small (see Fig. 7, $H_2/D_{cry} = 1$), a weak melt convection and a flat solidification interface are predicted, indicating a stable growth condition. When $H_2/D_{cry} = 5$, a strong convection is predicted. The temperature profile varies significantly as the length of hot zone changes. Note that the traditional Bridgman system has the H_2/D_{cry} value much larger than 5. Fig. 9 shows the temperature profiles along the centerline when $H_2/D_{cry} = 5$, 2 and 1, respectively. From the results, the growth interface is close to the bottom edge of the adiabatic zone. This is due to that melt convection pushes the solidification interface downwards. Table 3 shows the maximum and minimum values of stream functions in three systems. It can be concluded that the strength of melt flow is reduced as the length of H_2 is reduced.

To examine the effect of the transition zone length H_{tr} on growth, the predicted temperature and stream function distributions are presented in Fig. 10 for the transition length of $H_{tr}/D_{cry} = 2.5$. Comparing with the baseline case shown in Fig. 7, it is found that the predicted temperature distribution and streamline change insignificant when H_{tr} increases. This can be seen more clearly in the temperature profiles along the centerline of crystal as shown in Fig. 11. It is, therefore, concluded that the size change of H_{tr} has a minor influence on temperature and velocity distributions when the lengths of H_2 and H_{ad} are fixed. Table 4 shows the maximum and minimum values of stream functions

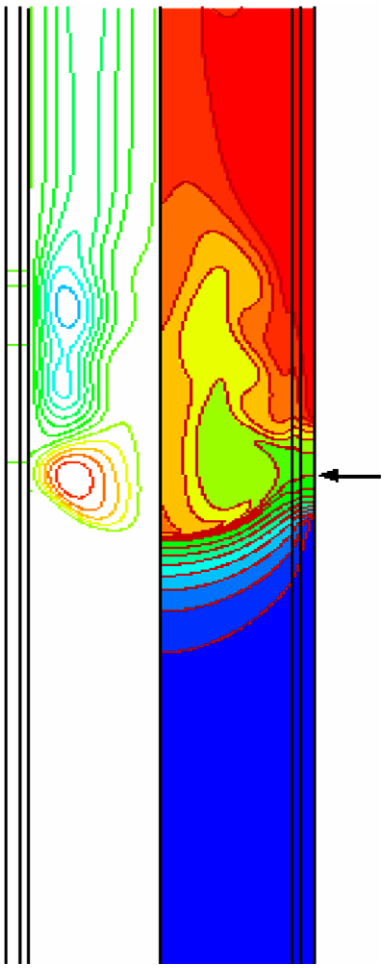

Fig. 6. The streamline (left half) and temperature (right half) distribution for the CdTe crystal with 38 mm in diameter.

for the above three cases. The strength of melt flow is similar for three cases.

To examine the effect of the adiabatic zone length H_{ad} on growth, the predicted temperature and stream function distributions are presented in Fig. 12 for the adiabatic length of $H_{ad}/D_{cry} = 2$. Fig. 13 presents the temperature profiles along the centerline of the crystal. It is seen that when the length of adiabatic zone increases, e.g., from $H_{ad}/D_{cry} = 1$ (Fig. 7) to 2 (Fig. 12), melt convection is weaken. It shall be noted that when the adiabatic zone length is cut to half from $H_{ad}/D_{cry} = 1$ to 0.5, the temperature distribution and streamline distributions seem to change not much. This result is quite surprising since the adiabatic length is considered to be important in determining temperature gradient in the melt. A short adiabatic length means a high temperature gradient in the melt. In the conduction case where the Grashof number is small, it is true that the length of the adiabatic region determines the temperature gradient since a virtually linear temperature profile is expected near the growth interface. However, when melt convection is strong, the temperature gradient in the melt is mainly determined by the thermal boundary layer of melt flow. The thickness of the boundary layer depends on the Grashof number and interface curvature. The length of adiabatic region in this case might play a minor role in the growth process for the short adiabatic zone. Of course, when the length of adiabatic region is long, the temperature gradient will be reduced and melt convection is weaken. Note that people may think that melt flow will be unstable if hot melt is sitting at the bottom and colder melt is sitting on

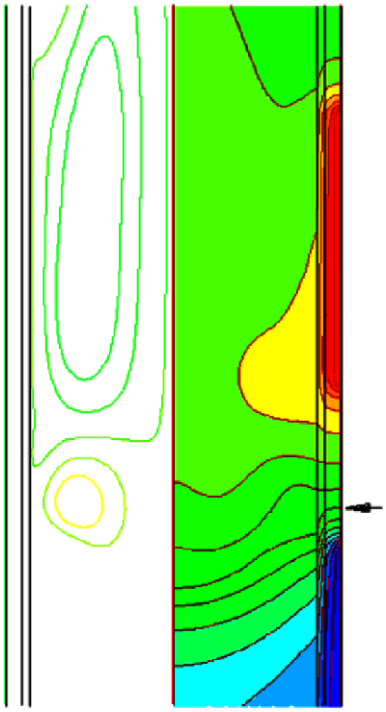

Fig. 7. Streamline and temperature distribution for the baseline case of the proposed InSb growth system with the crystal diameter of 38 mm. The system hot zone geometry is defined by $H_2/D_{cry} = 1$, $H_{tr}/D_{cry} = 0.5$ and $H_{ad}/D_{cry} = 1$. The Grashof number in the system is 3.2×10^6. The black arrow indicates the location of solidification interface with dimensionless temperature 0.0 and the interval of the isotherm lines is 0.125.

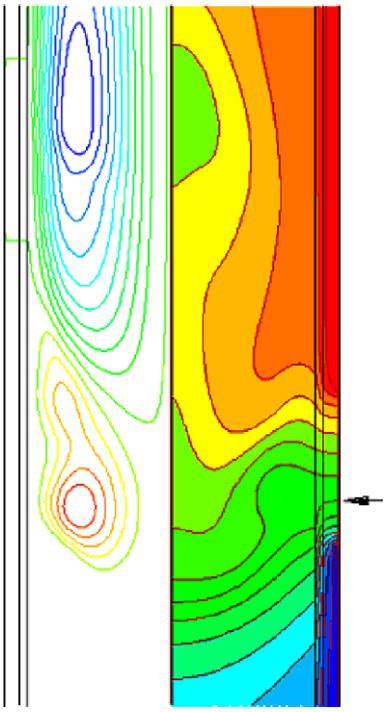

Fig. 8. Streamline and temperature distribution for the proposed InSb growth system with the crystal diameter of 38mm. The system hot zone geometry is defined by $H_2/D_{cry} = 5$, $H_{tr}/D_{cry} = 0.5$ and $H_{ad}/D_{cry} = 1$. The Grashof number in the system is 3.2×10^6. The black arrow indicates the location of solidification interface with dimensionless temperature 0.0 and the interval of the isotherm lines is 0.125.

the top for the proposed design. For the system proposed here, it is a tall liquid column with a lower sidewall temperature. The hot

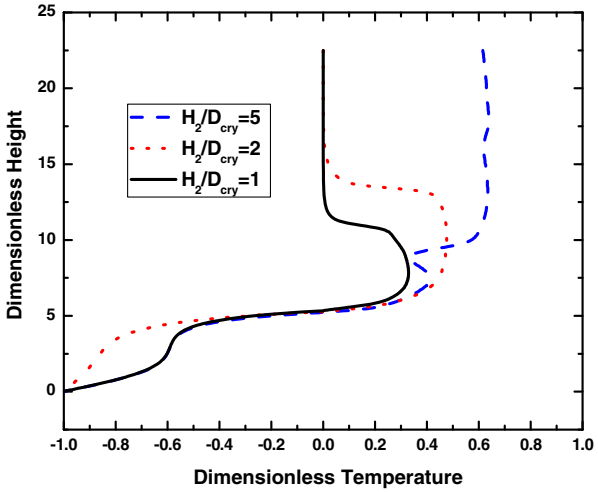

Fig. 9. Temperature profile along the centerline of a 38 mm InSb ingot with different H_2.

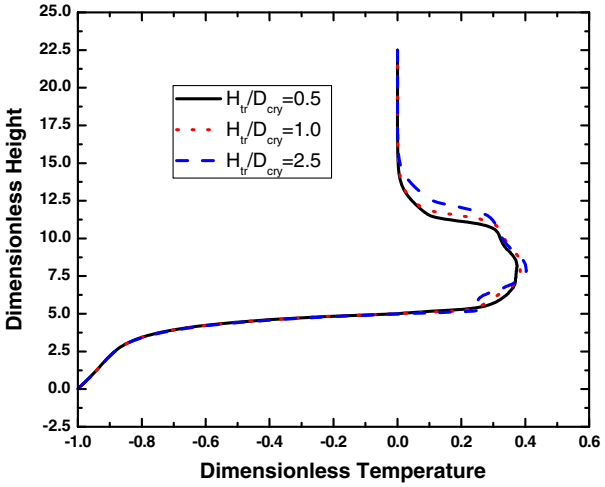

Fig. 11. Temperature profile along the centerline of a 38 mm with different H_{tr}.

Table 3
Minima and maxima of stream function with different H_2.

	H_2/D_{cry} = 5	H_2/D_{cry} = 2	H_2/D_{cry} = 1
Ψ_{max}	104.9	49.3	49.2
Ψ_{min}	−192.5	−84.8	−55.7
$\Psi_{max}-\Psi_{min}$	297.4	134.1	104.9

Table 4
Minima and maxima of stream function with different H_{tr}.

	H_{tr}/D_{cry} = 2.5	H_{tr}/D_{cry} = 1.0	H_{tr}/D_{cry} = 0.5
Ψ_{max}	76.0	67.7	83.0
Ψ_{min}	−76.2	−57.3	−54.3
Ψ_{max}-Ψ_{min}	152.2	125.0	137.3

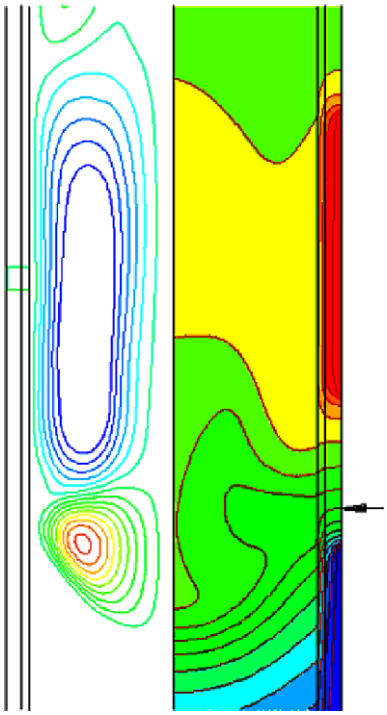

Fig. 10. Streamline and temperature distribution for the proposed InSb growth system with the crystal diameter of 38mm. The system hot zone geometry is given as H_2/D_{cry} = 1, H_{tr}/D_{cry} = 2.5 and H_{ad}/D_{cry} = 1. The Grashof number in the system is 3.2×10^6. The black arrow indicates the location of solidification interface with dimensionless temperature 0.0 and the interval of the isotherm lines is 0.125.

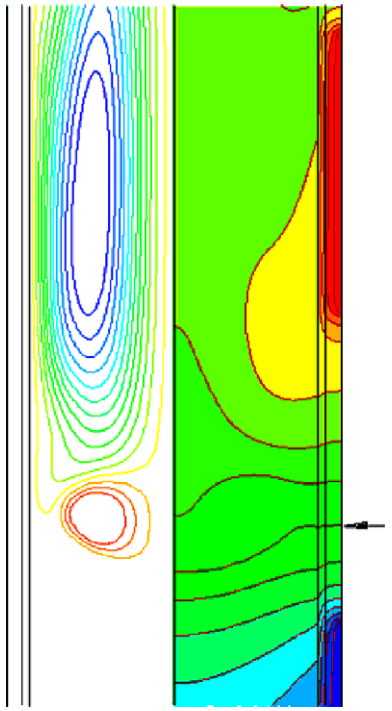

Fig. 12. Streamline and temperature distribution for the proposed InSb growth system with the crystal diameter of 38mm. The system hot zone geometry is defined by H_2/D_{cry} = 1, H_{tr}/D_{cry} = 0.5 and H_{ad}/D_{cry} = 2. The Grashof number in the system is 3.2×10^6. The black arrow indicates the location of solidification interface with dimensionless temperature 0.0 and the interval of the isotherm lines is 0.125.

melt cannot penetrate into the lower temperature region in depth. The flow is, therefore, restricted to the second hot zone. The simulation results show that the flow is weak and melt flow is stable.

Table 5 shows the maximum and minimum values of stream functions for three cases. The strength of melt flow is reduced slightly as H_{ad} is reduced.

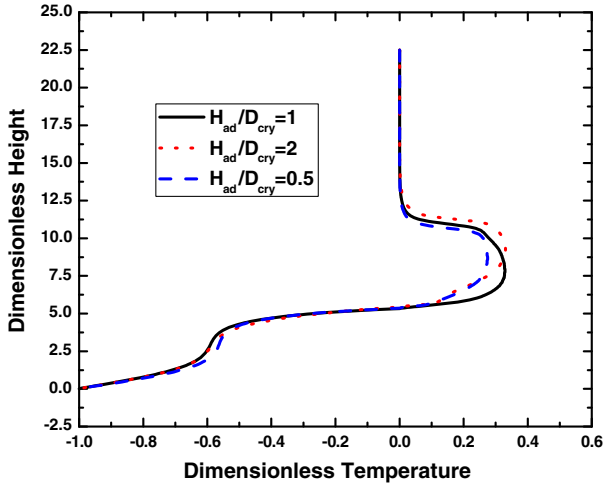

Fig. 13. Temperature profile along the centerline with different H_{ad}.

Table 5
Minima and maxima of stream function with different H_{ad}.

	H_{ad}/D_{cry} = 2	H_{ad}/D_{cry} = 1	H_{ad}/D_{cry} = 0.5
Ψ_{max}	30.9	49.2	17.6
Ψ_{min}	−77.9	−55.7	−76.1
Ψ_{max}-Ψ_{min}	108.8	104.9	93.7

5. Conclusions

The effects of Prandtl, Grashof, Stefan and Biot numbers on the melt flow field, axial temperature profile, and interface shape are investigated. It is found that the influence of melt flow on temperature distribution is strong when the Prandtl number is large. For a material with high Prandtl and high Grashof numbers, the temperature field and growth interface will be influenced significantly by melt convection, resulting in complicated temperature distribution and curved interface shape. Through calculated dimensionless parameters, the Prandtl, Grashof, Biot, and Stefan numbers, the effect of melt convection on curvature of the solidification interface have been determined and the strategic plan can be made for the proper use of melt flow enhancement/suppression.

A new design is proposed through reducing the length of the primary hot zone to suppress natural convection. Numerical results show that natural convection is significantly suppressed and temperature perturbation is decreased near the growth interface in the new growth system. Parametric studies are performed to investigate the effect of geometry size of different zones on crystal growth. Simulation results prove that natural convection is suppressed when the length of hot zone H_2 is reduced, and the length of transition zone, however, has less influence on melt convection and temperature distribution. Simulation results can provide help to optimize the growth system.

Acknowledgments

The work is supported by the NSF under the Grant No. CBET 0650604. Zheng and Zhang appreciate the financial support from Tsinghua University through the program of "Recruitment of Hundreds Outstanding Scientist".

References

[1] N. Ma, J.S. Walker, A parametric study of segregation effects during vertical Bridgman crystal growth with an axial magnetic field, J. Cryst. Growth 208 (1–4) (2000) 757–771.
[2] D.F. Bliss, R.M. Hilton, J.A. Adamski, MLEK crystal growth of large diameter (100) indium phosphide, J. Cryst. Growth 128 (1–4) (1993) 451–456.
[3] K.A. Kokh, V.N. Popov, A.E. Kokh, B.A. Krasin, A.I. Nepomnyaschikh, Numerical modeling of melt flows in vertical Bridgman configuration affected by a rotating heat field, J. Cryst. Growth 303 (1) (2007) 253–257.
[4] C. Martinez-Tomas, V. Munoz, CdTe crystal growth process by the Bridgman method: numerical simulation, J. Cryst. Growth 222 (3) (2001) 435–451.
[5] D.H. Kim, P.M. Adornato, R.A. Brown, Effect of vertical magnetic field on convection and segregation in vertical Bridgman crystal growth, J. Cryst. Growth 89 (2–3) (1988) 339–356.
[6] A.G. Ostrogorsky, Single-crystal growth by the submerged heater method, Meas. Sci. Technol. (1) (1990) 463–464.
[7] A.M. Marchenko, V.D. Golyshev, S.V. Bykova, Investigation of CdZnTe composition inhomogeneity at crystal growth by AHP-method, J. Cryst. Growth 303 (2007) 193–198. 2007.
[8] A.G. Ostrogorsky, G. Muller, Normal and zone solidification using the submerged heater method, J. Cryst. Growth 137 (1–2) (1994) 64–71.
[9] A. Fedyushkin, N. Bourago, V. Polezhaev, E. Zharikov, The influence of vibration on hydrodynamics and heat-mass transfer during crystal growth, J. Cryst. Growth 275 (1–2) (2005) e1557–e1563.
[10] L. Lun, A. Yeckel, P. Daoutidis, J.J. Derby, Decreasing lateral segregation in cadmium zinc telluride via ampoule tilting during vertical Bridgman growth, J. Cryst. Growth 291 (2) (2006) 348–357.
[11] A. Yeckel, G. Compere, A. Pandy, J.J. Derby, Three-dimensional imperfections in a model vertical Bridgman growth system for cadmium zinc telluride, J. Cryst. Growth 263 (1–4) (2004) 629–644.
[12] D. Vizman, I. Nicoara, G. Muller, Effects of temperature asymmetry and tilting in the vertical Bridgman growth of semi-transparent crystals, J. Cryst. Growth 212 (1–2) (2000) 334–339.
[13] C.W. Lan, Flow and segregation control by accelerated rotation for vertical Bridgman growth of cadmium zinc telluride: ACRT versus vibration, J. Cryst. Growth 274 (3–4) (2005) 379–386.
[14] Y.C. Liu, W.C. Yu, B. Roux, T.P. Lyubimova, C.W. Lan, Thermal-solutal flows and segregation and their control by angular vibration in vertical Bridgman crystal growth, Chem. Eng. Sci. 61 (23) (2006) 7766–7773.
[15] W.C. Yu, Z.B. Chen, W.T. Hsu, B. Roux, T.P. Lyubimova, C.W. Lan, Effects of angular vibration on the flow, segregation, and interface morphology in vertical Bridgman crystal growth, Int. J. Heat Mass Transfer 50 (1–2) (2007) 58–66.
[16] Y.C. Liu, B. Roux, C.W. Lan, Effects of cycle patterns of accelerated crucible rotation technique (ACRT) on the flows, interface, and segregation in vertical Bridgman crystal growth, Int. J. Heat Mass Transfer 50 (25–26) (2007) 5031–5040.
[17] H. Zhang, M.K. Moallemi, A multizone adaptive grid generation technique for simulation of moving and free boundary problems, Numer. Heat Transfer Part B 27 (1995) 255–276.
[18] H. Zhang, M.K. Moallemi, V. Prasad, A numerical algorithm using multizone grid generation for multiphase transport processes with moving and free boundaries, Numer. Heat Transfer Part B 29 (1996) 399–421.
[19] L.L. Zheng, D.J. Larson Jr., H. Zhang, Revised form of Jackson-Hunt theory: application to directional solidification of MnBi/Bi eutectics, J. Crystal Growth 209 (2000) 110–121.
[20] Y. Ma, L.L. Zheng, D.J. Larson, Microstructure formation during BiMn/Bi eutectic growth with applied alternating electric fields, J. Crystal Growth 262 (1–4) (2004) 620–630.
[21] H. Zhang, D.J. Larson, C.L. Wang, T.H. Chen, Kinetics and heat transfer of CdZnTe Bridgman growth without wall contact, J. Cryst. Growth 250 (1–2) (2003) 215–222.
[22] H. Zhang, L.L. Zheng, D.J. Larson, V. Prasas, Local and global simulations of Bridgman and Czochralski crystal growth, J. Heat Transfer 120 (1998) 865–873.
[23] V.M. Glozov, S.N. Chizhevskaya, Liquid Semiconductors, Plenum Press, New York, 1969.
[24] N. Shin, H. Taketoshi, Thermal conductivity of GaSb and InSb in solid and liquid states, J. Appl. Phys. 68 (10) (1990) 5125–5127.
[25] H. Lee, A.J. Pearlstein, Interface shape and thermally-driven convection in vertical Bridgman growth of gallium selenide: a semiconductor with aisotropic solid-phase thermal conductivity, J. Heat Transfer, Trans. ASME 123 (2001) 729–740.
[26] O. Madulung, Semiconductors Group IV Elements and III–V Compounds, Springer-Verlag, Berlin, 1991.
[27] W.J. HoweLL, M.M. Alger, C.A. Eckert, Application of the Lcpt model to solid–liquid equilibria for binary compound-forming alloys, Aiche J. 39 (9) (1993) 1519–1526.
[28] T. Maekawa, Y. Sugiki, S. Matsumoto, S. Adachi, S. Yoda, K. Kinoshita, Numerical analysis of crystal growth of an InAs-GaAs binary semiconductor by the Travelling Liquidus-Zone method under microgravity conditions, Int. J. Heat Mass Transfer 47 (21) (2004) 4535–4546.

[29] R. Bowers, R.W. Ure, J.E. Bauerle, A.J. Cornish, InAs and InSb as thermoelectric materials, J. Appl. Phys. 30 (6) (1959) 930–934.
[30] E.I. Rogacheva, N.I. Sinelik, I.M. Krivulkin, Semiconductor physics, Quant. Electron. Optoelectron. 5 (2002).
[31] C. Marin, A.G. Ostrogorsky, Bulk growth of quasi-binary quaternary alloys, J. Cryst. Growth 211 (1–4) (2000) 194–201.
[32] E.I. Rogacheva, I.M. Krivulkin, Proc. SPIE 277 (1997) 3182.